Assessing Fiber dispersion of FRCs Using an Image Processing Technique

Bang Yeon Lee[1], Yun Yong Kim[2], and Jin-Keun Kim[3]

[1] *Department of Civil and Environmental Engineering, Korea Advanced Institute of Science and Technology, Daejeon 305-701, Republic of Korea, ekvm80@kaist.ac.kr*
[2] *Department of Civil Engineering, Chungnam National University, 220 Gung-dong, Yuseong-gu, Daejeon, 305-764, Republic of Korea, yunkim@cnu.ac.kr*
[3] *Department of Civil and Environmental Engineering, Korea Advanced Institute of Science and Technology, Daejeon 305-701, Republic of Korea, kimjinkeun@kaist.ac.kr*

ABSTRACT

The fiber dispersion performance in fiber-reinforced cementitious composites is a crucial factor with respect to achieving desired mechanical performance. However, evaluation of the fiber dispersion performance in the composite PVA-ECC (Polyvinyl alcohol-Engineered Cementitious Composite) is extremely challenging because of the low contrast of PVA fibers with the cement-based matrix. In the present work, a new evaluation technique is developed and demonstrated. Using a fluorescence technique on PVA-ECC, PVA fibers are observed as green dots in the cutting plane of the composite. After capturing the fluorescence image with a Charged Couple Device (CCD) camera through a microscope, the fiber dispersion is evaluated using image processing and statistical tools. In the image processing step, the fibers are more accurately detected by employing a series of processes based on categorization, watershed segmentation, and morphological reconstruction. Test results showed that the dispersion coefficient α_f was calculated reasonably and the fiber detection performance was enhanced.
Keywords: FRCs, fiber dispersion, morphological reconstruction, watershed segmentation.

INTRODUCTION

Synthetic fibers have been used to improve the toughness of quasi-brittle cement-based materials such as concrete and mortar (Li, et al. 2001). Recently developed ultra-ductile Engineered Cementitious Composite (ECC) is an example of application of this approach (Li, et al. 2002, Kim, et al. 2003, Kim, et al. 2007). ECC is a micromechanically designed cementitious composite that is able to exhibit extreme tensile strain capacity (typically more than 2%) while

requiring only a moderate amount of fibers (typically less than 2% in a volume fraction). Since the fibers can bridge micro-cracks, the dispersion of fibers strongly influences the resulting mechanical performance of the composite.

Several techniques, including image analysis and transmission X-ray photography, are available for evaluating the fiber dispersion in a composite, i.e., determining the degree to which the fibers are homogeneously dispersed in the composite. These are mostly applicable to non-organic fibers such as steel or glass fibers. Recently, Ozyurt et al. (2006) proposed a nondestructive technique using AC-impedance spectroscopy; however, this approach is useful only for conductive fibers including steel and carbon fibers.

To date, the evaluation of organic/non-conducting fiber dispersions has seen little attention. The key step in evaluating an organic fiber dispersion is the fiber detection, since the contrast of organic fibers with cementitious materials is too low to allow detection in the composite. To overcome this obstacle, a fluorescence technique has been employed to specifically detect polyvinyl alcohol (PVA) fibers using their fluorescent characteristics.

Torigoe et al. (2003) suggested a new evaluation technique for PVA fiber dispersions. After capturing a fluorescence image with a Charged Couple Device (CCD) camera through a microscope, the image is divided into small units of appropriate pixel size. The degree of fiber dispersion is then calculated based on the deviation from the average number of fibers in a unit, which is obtained by a rigorous process of directly counting the fibers point by point. In addition, the distribution coefficient, which represents the degree of fiber dispersion, significantly depends on the size of the unit.

In the present work, the authors describe a new image processing to eliminate both the rigorous, manual fiber-counting processes and the undesirable impact of the unit size on the distribution coefficient. In the development of the proposed technique, the fiber detection performance is enhanced by employing categorization, a watershed algorithm, and morphological reconstruction.

FIBER DISPERSION EVALUATION TEHCNIQUE

Specimen preparation and image acquisition

The PVA-ECC specimen was produced on the basis of micromechanical principles (Li, et al. 2001) and then cured in water at 20±3 °C for 28 days. The specimen was cut with a diamond saw to obtain samples for fiber dispersion evaluation. Each sample, a rectangular block with a size of 13×36×20 mm, was polished to create a smooth surface on the exposed cross-section, i.e., the cutting plane. The polished surface was then photographed using image acquisition equipment, i.e., a fluorescence microscope (Olympus, BX51), a CCD camera, and image processing software. To obtain a digital image, the sample surface was first illuminated by a mercury lamp, followed by capture of a fluorescent image using a CCD digital camera through a GFP filter under 40×magnification.

Image processing for evaluation of fiber dispersion

As described in the previous section, the greenish points represent PVA fibers in the fluorescence image. The PVA fibers, therefore, should be easily detected by segmentation from the background image. The degree of fiber dispersion is then quantitatively evaluated based on calculation of a distribution coefficient αf, referred to as the fiber dispersion coefficient, as

expressed by Eq. (1) as follows (Kobayashi, et al. 1981).

$$\alpha_f = \exp\left[-\sqrt{\frac{\sum(x_i - 1)^2}{n}}\right] \quad (1)$$

where n is the total number of fibers on the image and denotes the number of fibers in the i-th unit, which is a square portion allocated to the i-th fiber on the assumption that the fiber dispersion is perfectly homogeneous. The fiber dispersion coefficient α_f is automatically calculated via the following steps.

(1) Convert the RGB image to a grayscale image;
(2) Convert the grayscale image to a binary image based on a set threshold – object detection based on a thresholding algorithm (Otsu, 1979);
(3) Divide the binary image into units, i.e., equivalent squares, of which the total number equals the number of fibers (n);
(4) Obtain the coordinate data for the centroid of each fiber image; and
(5) Count the number of fibers (x_i) located in each unit.

Following the initial two steps of the image processing, a composite image (Figure 1) can be obtained by combining the original grayscale image with the detected binary image. As indicated in Figure 1, fiber images of A, B, and C show quite different shapes in terms of aspect ratio, i.e., length-to-width ratio. This is attributed to the angle created between the fiber orientation and the sawed plane of the sample. In addition, the fiber images of B and D in Figure 1 reveal a single fiber whereas in reality it is composed of several fibers in close proximity; therefore, further improvement needs to be made to this thresholding algorithm in order to obtain a more accurate dispersion coefficient.

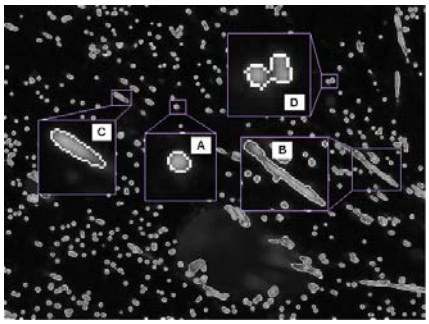

Figure 1. Combining original grayscale image with detected binary image

IMAGE PROCESSING FOR ENHANCING FIBER DETECTION PERFORMANCE

As discussed in the previous section, some improvements need to be made regarding the fiber-detection performance of the proto-type process to detect aggregate fiber images correctly.

To this end, an additional process was developed and inserted between step (2) and step (3) (described in the previous section). The added process basically consists of two parts. In the first part, fiber images are categorized into correctly detected single fiber images and aggregate fiber images, which are subdivided into several types, dependent on the shape of image. In the second step, aggregate fiber images are divided into individual fiber images using morphological reconstruction and watershed segmentation.

Categorization of fiber images

The first process entails categorizing fiber images into correctly detected single fibers and potentially aggregate fibers detected as a single fiber (Figure 2). In this process, we employed a watershed segmentation algorithm (Vincent, et al. 1991) to examine whether a single fiber image detected by the proto-type thresholding algorithm exhibits one segmented object, i.e., a single fiber. Table 1 compares the number of segmented objects with the number of fibers that are obtained from the thresholding algorithm and observations of the fluorescence image. If an image shows a single segmented object, the image is classified as a 'Single fiber,' denoted as Type S1. The fiber images categorized into Type S1 are correctly detected images; therefore, an additional process is not necessary.

Other types of fiber images correspond to cases where the number of objects segmented by the watershed algorithm is more than two. Typical fiber images are classified into four types, i.e., N1 (or S1), N2, N3, and N4, as illustrated in Figure 3. Four-type categorization, denoted as 1, 2, 3 and 4, is basically established according to the shape characteristics of the image.

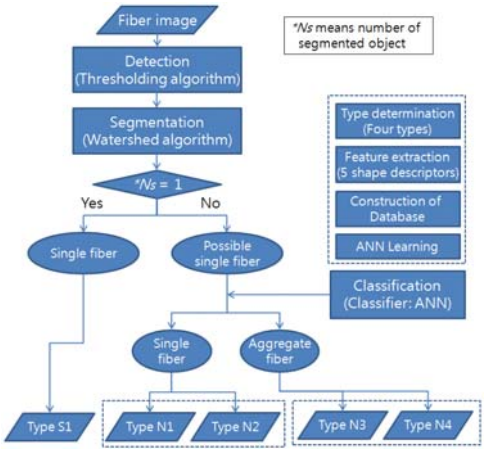

Figure 2. Proposed classification system

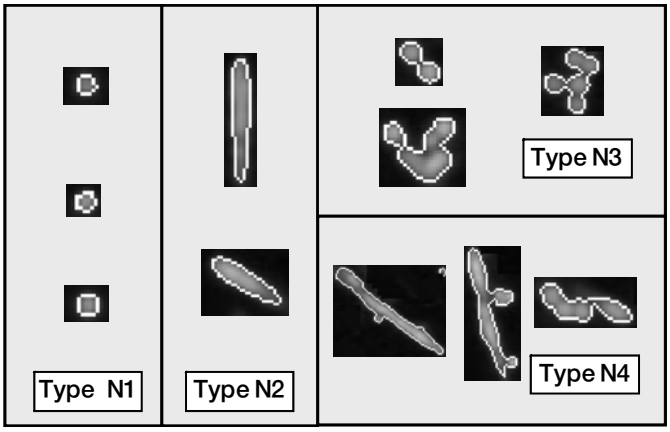

Figure 3. Typical fiber images

Type N1 and Type N2 represent single fiber images that are incorrectly over-segmented (Beucher, 1991) by the watershed algorithm, while these fibers are most likely single fibers based on close observation of the fluorescence image. Therefore, an additional process (i.e. beyond the proto-type algorithm) is not required for these two types of fiber images. In terms of the object's shape, Type N1 represents single fiber images whose shape is roughly circular. In contrast, Type N2 includes images of single fibers oriented at roughly right angles to the cutting plane; therefore, these appear highly elongated.

On the other hand, Type N3 and Type N4 represent aggregate fiber images incorrectly

detected as a single fiber by the thresholding algorithm. Type N3 mainly corresponds to simply aggregated fibers; thus, they are incorrectly detected as a single fiber. Type N4 represents aggregate fiber images lined up in succession and oriented at diverse angles to the cutting plane; therefore, they are easily over-segmented because of regional minima and maxima in the watershed segmentation process.

The second process entails feature extraction. The goal of feature extraction is to characterize an object to be recognized by measurements whose values are very similar for objects in the same category and very different for objects in different categories as well as to reduce the dimensions of the inputs. The potential features in images include color, texture, shape, and position of the objects. The shape is the most useful feature for classifying the fiber images since the other features, i.e., color, texture and position, are not suitable due to undistinguishable color/texture between objects and meaningless position of an object. The shape feature should be invariant to irrelevant transformations such as translation, scaling, rotation, and illumination change. We employed basic shape descriptors, such as object area (A_{ob}), convex hull area (A_{ch}), circumscribed circle area (A_{cc}), perimeter (l_p), and major axis length(l_l) of the object. However, direct use of these descriptors is not appropriate since these are not invariant to scaling, while they are invariant to translation and rotation. Therefore, five descriptors invariant to translation, rotation, and scaling are extracted to classify the fiber images into four types.

The first feature is solidity F_s, which is defined as the division of an object's area by that of the convex hull of an object, as expressed by Eq. (2). This feature can be used to effectively distinguish Type N1 and Type N2 fibers from other types.

$$F_s = \frac{A_{ob}}{A_{ch}} \tag{2}$$

The second feature is packing density F_c, which is defined as the division of an object's area by that of the object's circumscribed circle, as expressed by Eq. (3). This feature implies how circular the object is, effectively distinguishing Type N1 from others.

$$F_c = \frac{A_{ob}}{A_{cc}} \tag{3}$$

The value for F_c tends toward 0 for an extremely elongated object. F_c is also useful for calculating the inclined angle of the fiber to the cutting plane, as expressed by Eq. (4).

$$F_c = \frac{\pi dl/4}{\pi l^2/4} = \frac{d}{l} = \frac{d}{d/\cos\theta} = \cos\theta \tag{4}$$

where θ, d, and l are the inclined angle of the fiber, the diameter of the fiber, and the major axis length of the fiber image, respectively.

The third feature is F_p, which is defined as the division of an object's perimeter by its area, as expressed by Eq. (5). This feature can be used to effectively distinguish Type N3 from the other types.

$$F_p = \frac{l_p}{A_{ob}} \tag{5}$$

The other features are F_l and F_{rl}, which are defined as the division of the major axis length of the object by A_{ob} and l_{avg} (average value of all the major axis lengths of all fiber images), as expressed by Eq. (6) and Eq. (7), respectively. These features (F_l and F_{rl}) are useful for distinguishing elongated objects (Type N2 and Type N4) from others.

$$F_l = \frac{l_l}{A_{ob}} \tag{6}$$

$$F_{rl} = \frac{l_l}{l_{avg}} \tag{7}$$

Artificial neural networks are interconnected groups of artificial neurons that use a mathematical model for information processing based on a connectionist approach to computation. Thus, information or knowledge is represented by massive cross-weighted interconnections through training of a given database.

If artificial neural networks have not being trained concurrently or use an unchangeable database, their architecture can be optimized according to the given database representing a type of knowledge, so called "knowledge-based structuring." The capability of solving problems of artificial neural networks is determined by the complexity of the networks, which in turn may be determined by the number of layers, the complexity of neurons, the dynamic range of interconnections (weights and biases), and the number of hidden nodes. In general, the optimum architecture of an artificial neural network is realized by matching the complexity of the neural network to the complexity of the problem.

Hecht-Nielsen (1989) and Barron (1993) provide a proof that one hidden layer of neurons (operating sigmoidal activation functions) is sufficient to model any solution surface of practical interest. Therefore, one hidden layer is used in this study. Moody and Yarvin (1992) have compared the performance of several transfer functions and concluded that the sigmoidal transfer functions performed better than other functions, particularly when the data were noisy and contained non-linear relationships. Therefore, the hyperbolic tangent sigmoid function and the linear function are used as transfer functions on hidden neurons and output neurons, respectively.

Weights and biases are determined automatically by the training process. The Levenberg-Marquardt algorithm with weight decay (Krogh and Hertz, 1992) is adopted as a learning algorithm in order to prevent over-fitting.

In order to determine the number of hidden nodes, a 10-fold cross-validation method is adopted, wherein networks having different numbers of hidden nodes are trained. The network having the best performance, that is, the case where the accuracy on the test sets is the maximum, is then selected. This process is repeated 10 times so as to minimize the effect of the initial values of weights and biases for each fold data set. Five features are used as input parameters. Figure 4 shows the accuracy on the training sets and test sets versus the number of hidden nodes. The optimum network architecture is accordingly found to be 5-4-4 (number of neurons in input

layer, 5; number of neurons in hidden layer, 4; and number of neurons in output layer, 4); i.e., this architecture yielded the maximum accuracy on the test sets. The artificial neural network that will be used for the classification of fiber images is trained using the whole database. The accuracy of the artificial neural network on the basis of a jack-knife validation is 95.3%.

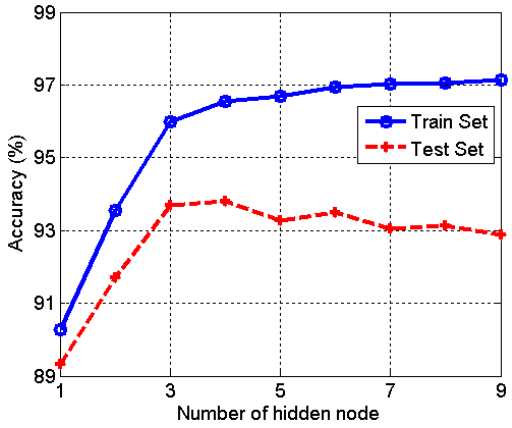

Figure 4. Performance on the training sets and test sets versus number of hidden nodes

Detection of aggregate fiber images (Type N3 and Type N4)

In order to correctly detect an aggregate fiber image (Type N3 and Type N4), a watershed segmentation algorithm and morphological reconstruction algorithm were employed in the present study.

To correctly detect Type N3 and Type N4, a watershed segmentation algorithm was adopted. Currently, watershed transformation is a widely used technology in image segmentation. Watershed segmentation can be implemented on the basis of a drainage analogy or immersion analogy. The drainage analogy concept is based on an analogy that all points on a surface are classified according to drainage. First, a downstream path from each pixel of the image to the local minima of the image surface altitude is found. A catchment basin is then defined as the set of pixels for which their respective downstream paths end up in the same altitude minimum. The watershed line, which represents the boundary between objects, is defined as the set of pixels except the catchment basin pixels. The immersion analogy concept, meanwhile, is based on an analogy that all points on a surface are classified according to filling and merging the catchment basins from the bottom. The water starts filling all catchment basins. If two catchment basins are about to merge, a high dam is built to prevent this. When all basins have been filled, the dams represent the watershed lines. In this study, a watershed segmentation algorithm based on the immersion analogy proposed by Vincent et al. (1991) was adopted.

Morphological reconstruction is adopted to minimize the over-segmentation problem caused by regional minima and maxima in the watershed segmentation process of Type N4. In the standard morphological reconstruction, a mask image (g) is reconstructed from a marker image (f) by iterating geodesic dilations of the marker image inside the mask image until stability is attained; i.e., the image no longer changes. Both of these images have the same size, and $f \leq g$. A mask image is the initial image that will be reconstructed and a marker image is created by subtracting a constant value (h) from the mask image. The number of fibers finally detected from Type N4 fibers is dependent on the value of h. In this study, *h* was determined to

be 20, empirically by the use of trial and error.

VALIDATION OF THE METHOD

To assess the validity of the proposed technique, a series of tests was performed on real and artificial fiber images. As shown in Figure 5, seven groups of fiber images were selected for closer examination. Figure 6 displays the detection test results, where the white point located on the grayscale image (fiber) indicates the center of the detected fiber image. A, B, C, and D fiber images in Figure 6, which were classified as Type N3 fibers, were more successfully detected using the enhanced detection process relative to the results of the proto-type process. Detection results of E, F, and G fiber images (Type N4) in Figure 6 are also indicative of significantly improved fiber-detection performance, where over-segmentation is minimized by applying the morphological reconstruction. All results in Figure 6(b) indicate that the enhanced detection process yields significantly improved fiber-detection performance.

Figure 7, in which the dispersions of (a) and (b) are perfect and severely biased, respectively, shows artificial fiber images tested to assess the validity of the α_f calculation. The test results demonstrate correct calculations, showing α_f values of 1.0 and 0.041 for each image (see Figure 8). α_f values calculated by the proto-type algorithm and the enhanced algorithm were 0.384 and 0.348, respectively. The enhanced algorithm provides lower α_f values, i.e. decreased by 9.4%, compared to the proto-type algorithm. This is most likely due to correct segmentation of the fibers from the aggregate fiber images, where the fibers are located in close enough proximity to decrease the average α_f for the same sample.

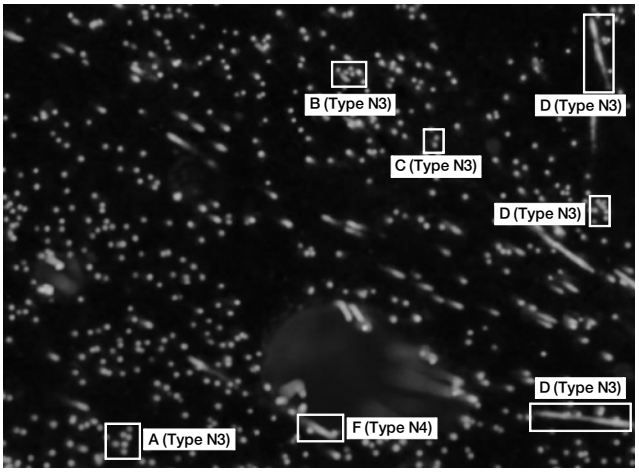

Figure 5. Seven groups of fiber images

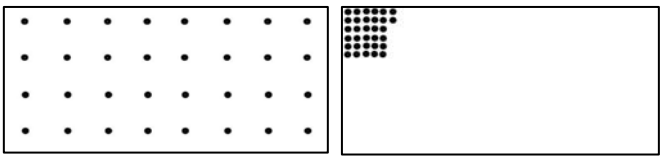

Figure 7 Artificial fiber images to test

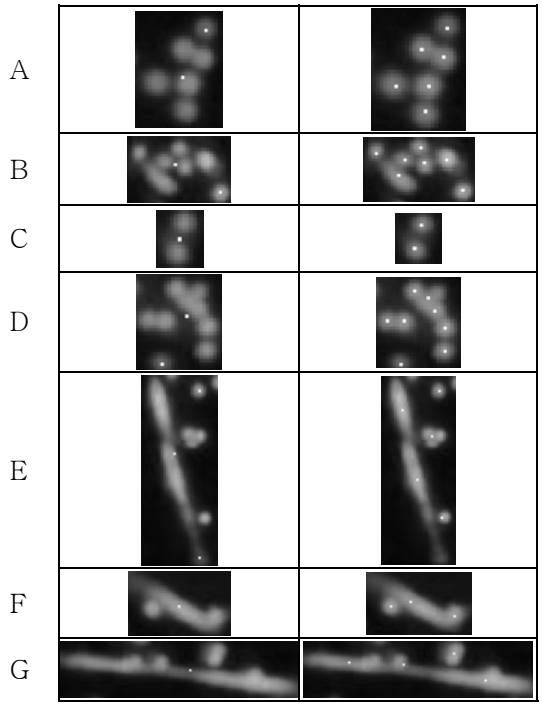

Figure 6. Test results

CONCLUSION

This paper proposes a new technique to evaluate the PVA fiber dispersion in Engineered Cementitious Composite. A series of experimental and analytical investigations was carried out to verify the validity of this technique. The following conclusions can be drawn from the current results:

(1) The proposed technique is essentially composed of stepwise tasks. First, the specimen is prepared and treated, followed by the acquisition of a fluorescence image. Based on the proposed image processing algorithm, the fiber images are then automatically detected in a binary image converted from the fluorescence image. A fiber dispersion coefficient α_f is finally calculated by a mathematical treatment performed on the image data.

(2) To enhance the fiber-detection performance, the fiber images detected by the proto-type thresholding algorithm were classified by a watershed segmentation algorithm into two categories, single fibers (Type S1) and possible single fibers (Type N family). The fibers in Type N family were then subdivided into four types (Type N1, N2, N3 and N4) by an ANN, which was carried out to enhance fiber-detection efficiency. For this process, five features, F_s, F_c, F_p, F_l and F_{rl}, which are invariant to image translation, scaling, and scaling, were extracted. For correct detection of aggregate fiber images (Type N3 and Type N4), the watershed segmentation algorithm and morphological reconstruction were adopted.

(3) The calculation accuracy of α_f was demonstrated by tests on artificial images. In addition, the results of real image tests indicated significant improvement of the fiber-detection performance. This was achieved by applying an enhanced detection algorithm, correctly separating fiber images from the aggregate image, and relieving the over-segmentation problem. It was also found that the enhanced detection process provided a lower average α_f compared to that of the proto-type process. This is because of correct segmentation of the fibers from aggregate fiber images, which are located in close enough proximity to decrease the average α_f for the same sample. On the other hand, the application of morphological reconstruction resulted in an increase of α_f, most likely due to correction of the over-segmentation error.

ACKONWLEDGEMENTS

The authors would like to thank the Infra-Structures Assessment Research Center funded by Korea Ministry of Construction and Transportation (MOCT) for financial support.

REFERENCES

Barron, A.R. (1993), “Universal approximation bounds for superpositions of a sigmoidal function”, *IEEE Trans of Inform Theory*, 39(3), 930-945.

Beucher, S. (1991) “The watershed transformation applied to image segmentation”, Conference on Signal and Image processing in Microscopy and Microanalysis, September, 299-314.

Hecht-Nielsen, R. (1989), “Theory of the backpropogation neural network”, In Proceedings of International Joint Conference on Neural Networks. Washington, D.C., USA: IEEE, V. I, 593-605.

Kim, J. K., Kim, J. S, Ha, G. J. and Kim, Y. Y. (2007), "Tensile and Fiber Dispersion

Performance of ECC (Engineered Cementitious Composites) Produced with Ground Granulated Blast Furnace Slag", *Cement and Concrete Research*, 37(7), 1096-1105.

Kim, Y. Y., Kong, H-J and Li, V. C. (2003), “Design of engineered cementitious composite suitable for wet-mixture shotcreting”, *ACI Materials Journal*,100(6),511-518.

Kobayashi, K. (1981), "Fiber reinforced concrete", Tokyo: Ohm-sha.

Krogh, A., Hertz, J.A. (1992), “A simple weight decay can improve generalization”, In: Moody JE, Hanson SJ, Lippmann RP, editors. Advances in Neural Information Processing Systems 4. Morgan Kaufmann Publishers, 950-957.

Li, V. C., Wang, S. and Wu, C. (2001), “Tensile strain-hardening behavior of polyvinyl alcohol-engineered cementitious composite (PVA-ECC)”, *ACI Materials Journal*; 98(6), 483-492.

Moody, J.E., Yarvin, N. (1992), “Networks with learned unit response functions”, In: Moody JE, Hanson SJ, Lippmann RP, editors. Advances in Neural Information Processing Systems 4. Morgan Kaufmann Publishers, 1048-1055.

Otsu, N.A. (1979), “Threshold Selection Method from Gray Level Histogram”, *IEEE Transactions on Systems, Man, and Cybernetics*, SMC-9(1), 62-66.

Ozyurt N, Woo LY, Mason TO, and Shah SP. Monitoring Fiber Dispersion in Fiber-Reinforced Cementitious Materials: Comparison of AC-Impedance Spectroscopy and Image Analysis. ACI Mater J 2006;103(5);340-347.

Torigoe, S., Horikoshi, T., and Ogawa, A.(2003),"Study on evaluation method for PVA fiber distribution in engineered cementitious composite", *Journal of Advanced Concrete Technology*, 1(3), 265-268.

Vincent, L. (1993), "Morphological Grayscale Reconstruction in Image Analysis: Applications and Efficient Algorithms," *IEEE Transactions on Image Processing*, 2(2), April, 176-201.